IPPI

Polyolefins Journal, Vol. 5, No. 1 (2018)
DOI: 10.22063/POJ.2017.1879.1100

ORIGINAL PAPER

Role of covalent bond formation in morphology and properties of PP/PP-g-PS binary blends

Li Qian[1], Zhang Yongjie[2], Li Huayi[1*], Peng Zhongchuan[1], Zhang Yu[1], Hu Youliang[1]

[1]Beijing National Laboratory of Molecular Sciences, CAS Key Laboratory of Engineering Plastics, Joint Laboratory of Polymer Science and Materials, Institute of Chemistry, Chinese Academy of Sciences
No 2, 1st north street, zhongguancun, Beijing P.R. China
[2]Dalian Polytechnic University, 116034, Dalian P.R. China

Received: 25 May 2017, Accepted: 21 October 2017

ABSTRACT

PP-g-PS copolymer is a typical compatilizer used in polypropylene and polystyrene immiscible blends. PP-g-PS copolymers with different side chain lengths were synthesized, and their thermal and mechanical properties were characterized by differential scanning calorimetry (DSC), polarizing optical microscopy (POM) and dynamic mechanical analysis (DMA), respectively. The DSC and POM results show that the introduction of PS side chain dramatically accelerates the crystallization rate of the PP main chain due to the covalent bond in the PP and PS copolymer. Furthermore, the copolymers become more rigid as the PS component content increases. Blend of PP with PP-g-PS copolymer was prepared to investigate the compatibility between PP and PS. The properties of five PP/PP-g-PS binary blends were characterized by DSC, DMA, scanning electron microscopy (SEM) and mechanical testing. Well dispersion of PS and small PS particle size are detected in the binary blends. The formation of covalent bond between PP and PS also increases the compatibility and interfacial adhesion between these two phases. **Polyolefins J (2018) 5: 85-95**

Keywords: Polypropylene; polypropylene-graft-polystyrene; binary blends; covalent bond; morphology.

INTRODUCTION

Polypropylene (PP) is one of the most widespread commercial polymers due to its outstanding physical and chemical properties. The lack of toughness, strength and stiffness have limited its applications as an engineering plastic, so blending with rigid polymers or elastomers is commonly used to reinforce or toughen PP [1-5]. However, the blends usually accompany with immiscibility problems. An immiscible blend system usually exhibits phase segregation and low interfacial adhesion and, as a consequence, presents poor mechanical properties. Furthermore, it is reported that the interface adhesion and dispersed particle size have influenced the toughening efficiency significantly in many researches. Therefore, it is important to strength the interfacial adhesion and to control the dispersed particle size for immiscible blends.

---

* Corresponding Author - E-mail: lihuayi@iccas.ac.cn

PP and polystyrene (PS) blend is known as a typical immiscible system, and the compatibility between PP and PS is difficult to improve. Polypropylene-graft-polystyrene (PP-g-PS) is a typical compatibilizer for PP/PS blends to increase the phase adhesion, to reduce the interfacial tension, and to improve the morphology and mechanical properties of PP/PS alloys [6, 7]. Whereas, the compatibilization efficiency is affected by many factors, such as main chain length, side chain length, graft distributions, etc. [6-8]. In our previous work [9], PP-g-PS copolymers with various side chain lengths of PS sequences were synthesized and used as the compatibilizer of PP/PS blends, and it was found that the morphologies, crystallinity and glass transition temperatures of the PP/PP-g-PS/PS blends markedly depended on the side chain length of PP-g-PS copolymer. The PP main chain and PS side chain in the PP-g-PS graft copolymers are connected together with covalent bond. This covalent connecting structure is favorable for improving the interfacial adhesion of binary blends. Until now, few researches have focused on the binary blends of PP/PP-g-PS.

In this paper, PP-g-PS copolymers with low graft density were synthesized and their properties were characterized. Then, the synthesized PP-g-PS graft copolymers were blended into PP to form PP/PP-g-PS binary blends. The morphologies, crystallinity and mechanical properties of the PP/PP-g-PS binary blends were also investigated.

EXPERIMENTAL

Materials

Propylene (polymerization grade) and $AlEt_3$ were provided by Yanshan Petro-Chemical Co. and used without further purification. $MgCl_2$-supported $TiCl_4$ Ziegler-Natta catalyst (Ti: 3.38 wt.%) was kindly donated by Xiangyang Chemical Co. Potassium tert-butylate (tert-BuOK, 97%) and n-butyllithium (n-BuLi, 2.8 M in hexane) were purchased from Alfa Aesar and used without further purification. Toluene and hexane were dried by refluxing over sodium/benzophenone under an argon atmosphere and finally distilled before use. Styrene was stirred over CaH_2 and distilled under reduced pressure before use.

Propylene-co-p-allyltoluene (PP-co-p-AT) and PP-g-PS synthesis

The propylene-co-p-allyltoluene (PP-co-p-AT) and PP-g-PS copolymers were synthesized according to our previous work [9]. The isotactic polypropylene (M_n=109,400, M_w/M_n=3.6) was synthesized according to our previous work [10] using $MgCl_2$-supported Ziegler-Natta catalyst, $AlEt_3$ (1.8 M in hexane) and di-isopropyl dimethoxysilane (DIPDMS).

Polymer blending

The PP/ PP-g-PS blends were carried out at 190°C and 50 rpm in a Haake mixer with a blending time of 10 min. After blending, all the samples were cooled to room temperature in air. For the PP/ PP-g-PS blends, the weight ratio of PP to PP-g-PS was fixed at 97.5/2.5, 95/5, 92.5/7.5, 90/10, and 85/15, respectively. The compositions of the polymer blend samples are listed in Table 4.

NMR analysis

^{1}H NMR spectra were recorded on a Bruker DRX-400 spectrometer in the Fourier transform mode. The samples were measured at 380 K in tetrachloro-1, 2-dideuterioethane ($C_2D_2Cl_4$) which was also used as reference (δ (^{1}H) = 5.98 ppm) and lock.

DSC analysis

Differential scanning calorimetry (DSC) was performed on a TA Q2000 instrument. All the samples were first heated from room temperature to 200°C and held there for 2 min, immediately cooled down to -50°C at the rate of 20°C/min and then heated up again to 200°C at the rate of 20°C/min. The analysis was based on the second heating curve.

The isothermal crystallization was performed as follows. The samples, sealed in aluminum pans, were heated to 210°C, held there for 5 min to erase any thermal history and then cooled to the designated crystallization temperature in the range of 122-130°C for neat PP isothermal crystallization and 128-136°C for PP-g-PS graft copolymers isothermal crystallization at a rate of 50°C/min. The curves of heat flow as a function of time were recorded.

POM analysis

In the polarizing optical microscopy (POM) characterization, the film was heated to 210°C, held there for 5 min to eliminate any thermal history and then cooled to 140°C as quickly as possible for isothermal crystallization.

DMA analysis

The dynamic mechanical analysis (DMA) was performed on a TA instruments Q800 dynamic mechanical analyzer in conjunction with a liquid nitrogen cooling system. All samples were measured in the single cantilever mode from -50°C at a heating rate of 3°C/min. The amplitude was 25 lm and the frequency of deformation (oscillating frequency) was 1 Hz.

SEM analysis

The specimens which were molded for DMA analysis also were used in the scanning electron microscope (SEM) observation. The samples were fractured in liquid nitrogen. The fracture surfaces were coated with a thin layer of gold before SEM observation. The morphologies of the polymer blends were observed in a scanning electron microscope (SEM; JSM-6700F, JEOL, Tokyo, Japan). The dimension of the PS disperse phase was measured using Nano Measurer software.

Mechanical properties testing

Tensile and flexural testing were determined with a universal tester (Instron 1122, UK). The tensile properties of the specimens were measured in general accordance with ISO 527 at a crosshead speed of 50 mm/min; the flexural properties were determined in general accordance with ISO 178 at a crosshead speed of 2 mm/min. The impact strength was measured with an impact testing machine (CSI-137C, USA) in general accordance with ISO 180. The results were taken as an average value from measurements of at least five specimens.

RESULTS AND DISCUSSION

Structure and properties of PP-g-PS copolymer

The graft density (defined as the average number of grafted side chains per 1000 carbons in the PP backbones), weight ratio of styrene and propylene (WPS/PP), and graft length (GL, defined as the average degree of polymerization of PS sequences) were calculated in our previously work [9] by ^{1}H NMR spectra. The graft density of synthesized PP-g-PS copolymer is 0.94, and the other results are summarized in Table 1. The thermal characterization results of PP-g-PS copolymers are shown in Table 2. Theoretically, the graft copolymers should display two T_g values that belong to the PP backbone and the PS sequences, respectively. However, the PP-g-PS copolymers showed a constant T_g value of PS sequence at about 109°C, while the T_g of PP backbones below room temperature did not display clearly. As shown in Table 2, the melting temperature (T_m) values of synthesized graft copolymers are very close to that of neat PP at 164.7°C excepting for PGS1.

Table 1. Characterizations of the PP-g-PS copolymers.

Sample	$W_{PS/PP}$ $^{(a)}$	GL$^{(b)}$
PGS1	0.57	122
PGS2	0.90	193
PGS3	1.30	279
PGS4	1.70	365

$^{(a)}$ PS/PP weight ratio in the PP-g-PS copolymer, calculated by ^{1}H NMR spectra.
$^{(b)}$ Side chain length of PP-g-PS copolymer, calculated by ^{1}H NMR spectra.

To investigate the effect of side chain length on the crystallization morphology, the isothermal crystallization micrographs of neat PP and PP-g-PS copolymers at 140°C were carried out by POM analysis as shown in Figure 1.

Table 2. Thermal characterization results for PP-g-PS and neat PP.

Sample	$W_{PS/PP}$ $^{(a)}$	$T_{g,PS}$ (°C)	T_c (°C)	T_m (^{OC})
PP	0	-	100	164.7
PGS1	0.57	108.6	102	170.0
PGS2	0.90	109.5	112	165.4
PGS3	1.30	108.9	116	164.7
PGS4	1.70	108.5	113	164.2

$^{(a)}$ PS/PP weight ratio in the PP-*g*-PS copolymer, calculated by ^{1}H NMR spectra.

Within the scope of observation, the neat PP displays a typical spherulitic morphology with Maltese-cross pattern as well as the biggest crystal size. The graft copolymers show more de-

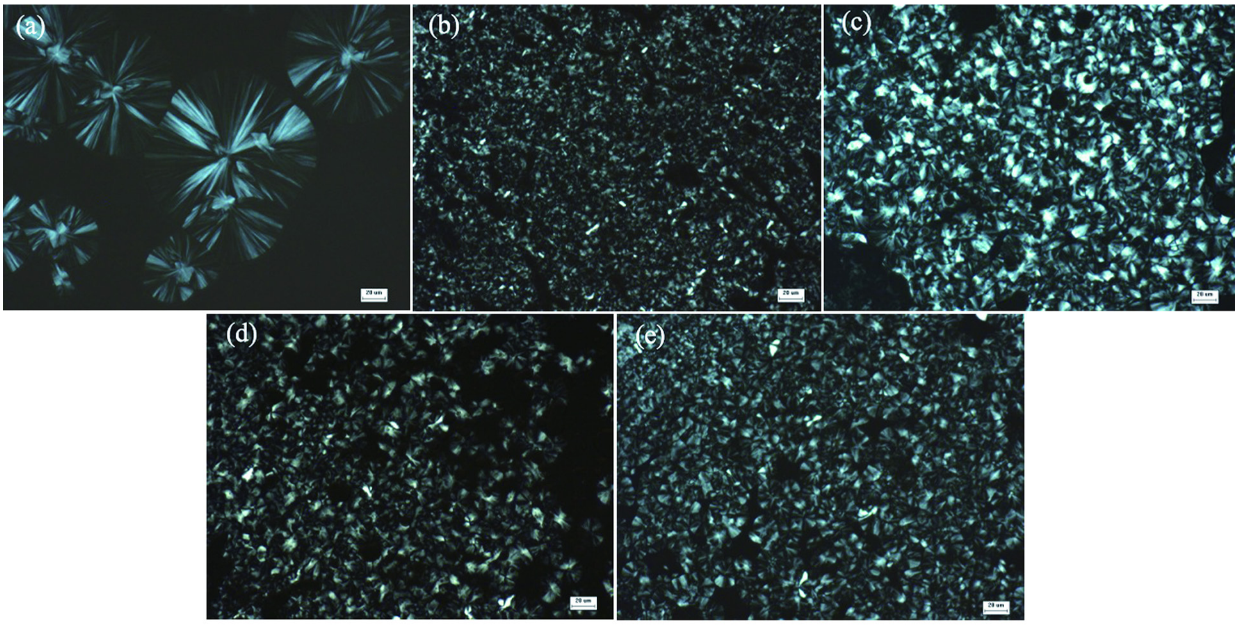

Figure 1. Optical micrographs of PP and PP-g-PS copolymers isothermally binary crystallized at 140oC, (a):PP, (b):PGS1, (c):PGS2, (d):PGS3, (e):PGS4.(the scale bar is 20μm).

fects than PP, and display obviously increasing crystal number and decreasing crystal size due to the folding problem of PS branch on the PP main chain. The reason of this phenomenon is that the microphase separation between PS- and PP-rich phase facilitated the crystallization process [11], and the PS particles had a heterogeneous nucleation effect on PP. In addition, PGS1 possesses obviously higher observed crystal number and smaller crystal size than the other three graft copolymers. It may be caused by the shorter branch length in PGS1.

The DSC and POM results display that PGS1 has a higher T_m, higher crystal number and smaller crystal size than the other copolymers and PP. Furthermore, the isothermal crystallization of neat PP and PP-g-PS copolymers were conducted. To analyze the isothermal crystallization of the graft copolymers, the well-known Avrami equation is used. The relative crystallinity of a polymer at time t, X_t, can be expressed as:

$$1-X_t=\exp\left(-kt^n\right) \tag{1}$$

where n is a constant value which depends on the mechanism of nucleation and the formation of crystal growth, and k is a rate constant containing the nucleation and growth parameters. The Avrami equation in the simple form represents unimpeded spherical crystal growth and required sigmoidal shape [12]. X_t is equal to the ratio of the heat generated at time:

$$X_t=\frac{\Delta H_c(t)}{\Delta H_c(\infty)}=\frac{\int_0^t \frac{dH_c(t)}{dt}dt}{\int_0^\infty \frac{dH_c(t)}{dt}dt} \tag{2}$$

where dH/dt is the rate of heat evolution. Figure 2 plots the X_t versus t curves of PP and graft copolymers at different crystallization temperatures. As shown, the time to reach the maximum degree of crystallinity in the five samples increases as the crystallization temperature elevating. The graft copolymers display about 10°C higher isothermal crystallization temperature than neat PP, but the times to reach the maximum degree of crystallinity are very close. Eq. (2) can be changed to:

$$\ln\left[-\ln\left(1-X_t\right)\right]=\ln k+n\ln t \tag{3}$$

Figure 3 represents that the curves of $\ln[-\ln(1-X_t)]$ versus lnt are approximately straight lines, which indicates that the isothermal crystallization behavior of PP and its graft copolymer obeys the Avrami equation. The Avrami exponent n and crystallization rate constant k determined from the slope and intercept of the line at different crystallization temperatures are illus-

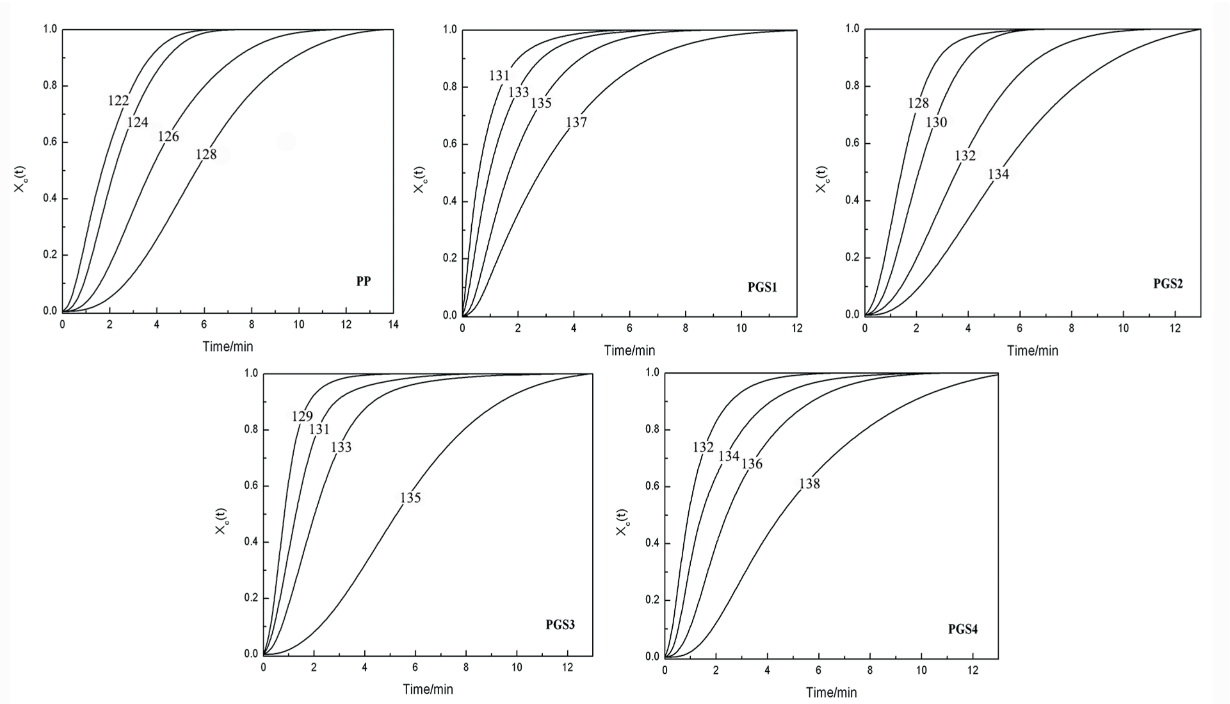

Figure 2. Development of relative crystallinity with time for isothermal crystallization of PP and PP-g-PS copolymers at different crystallization temperatures.

trated in Table 3, respectively. And the crystallization half-time ($t_{1/2}$) is calculated as follows:

$$t_{1/2} = \left(\ln 2 / k\right)^{1/n} \quad (4)$$

The $t_{1/2}$ results are also listed in Table 3. As shown, the $t_{1/2}$ value of graft copolymers at each crystallization temperature is less than that of neat PP even though the crystallization temperature is about 10°C higher. The result implies the crystallization process of PP-

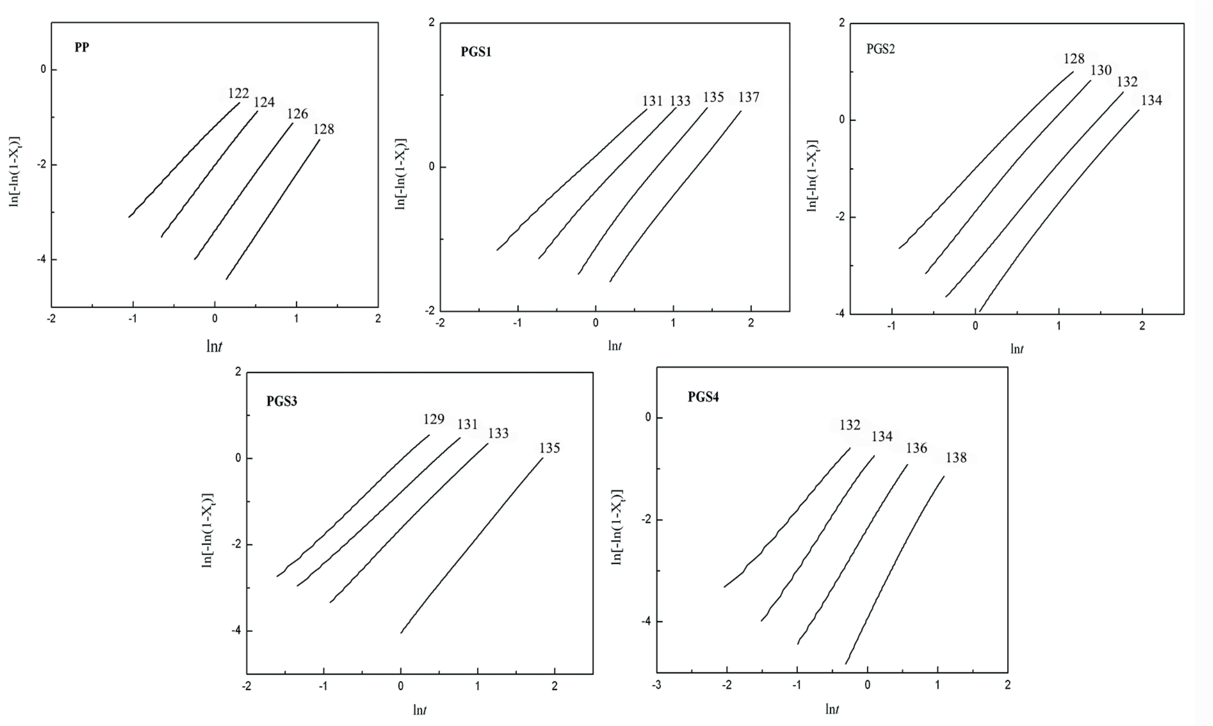

Figure 3. ln[−ln(1−X_t)] versus lnt curve of PP and PP-g-PS copolymers at different crystallization temperatures.

Table 3. Kinetic parameters of neat PP and PP-g-PS copolymers.

Sample	T_c(°C)	$t_{1/2}$(min)	n	ln*k*
PP	122 124 126 128	1.68 2.20 3.73 5.67	1.77 2.25 2.41 2.56	-1.20 -2.02 -3.38 -4.75
PGS1	131 133 135 137	0.58 0.97 1.67 2.77	1.00 1.13 1.34 1.39	0.16 -0.34 -1.08 -1.81
PGS2	128 130 132 134	1.40 2.08 3.54 5.22	1.77 2.00 2.00 2.12	-1.00 -1.87 -2.91 -3.87
PGS3	129 131 133 135	0.82 1.28 2.03 5.25	1.70 1.66 1.80 2.19	-0.05 -0.78 -1.64 -4.00
PGS4	132 134 136 138	0.92 1.44 2.40 4.52	1.60 2.05 2.28 2.65	-0.19 -0.90 -2.17 -3.92

g-PS is faster than that of neat PP, which is in accordance with the POM results. The nonintegral n value may reflect a mixed nucleation and crystal growth mechanism. The n values of pure PP, PGS2, PGS3, and PGS4 are fluctuated round 2.0. It can be inferred that the crystallization process of PP and the three graft copolymers were initiated by heterogeneous and homogeneous nucleation. However, the n value of the PGS1 graft copolymer is far below 2.0, which may be ascribed to the heterogeneous nucleation [13].

The dynamic mechanical properties of neat PP and PP-g-PS copolymers were detected by DMA. Figure 4 shows the temperature dependence of storage modulus (E′) and loss modulus (E″) for PP and the graft copolymers at a frequency of 1 Hz. As shown, the dynamic mechanical properties are changed drastically by the incorporation of PS branch sequences onto the PP backbones. Figure 4(a) displays that the E′ of graft copolymers are higher than that of PP in the range of 25~100°C. This result indicates that the rigidity of graft copolymers is higher than that of neat PP. As shown in Figure 4(b), two glass transition points belong to the PP backbone, and the PS sequences are observed. It implies that the copolymers possess a two-phase structure. And the DMA results are an effective complement to DSC on T_g. As shown, the glass transition temperature of PP backbones ($T_{g,PP}$) in the graft copolymer shifts toward lower temperature comparing with neat PP due to their shorter propylene repeat units than neat PP. And the glass transition temperature of the PS sequences ($T_{g,PS}$) elevates as the side chain length increasing until it reaches a constant $T_{g,PS}$ value.

PP/PP-g-PS blends

According to our previous research [9], suitable side chain length is favorable for the compatibility of PP/PS blends. Therefore, PGS2 with a graft length of 192 was chosen as a typical graft copolymer to blend with PP in different weight ratios. The morphologies and mechanical properties of the PP/PP-*g*-PS binary blends were also studied. The compositions of the

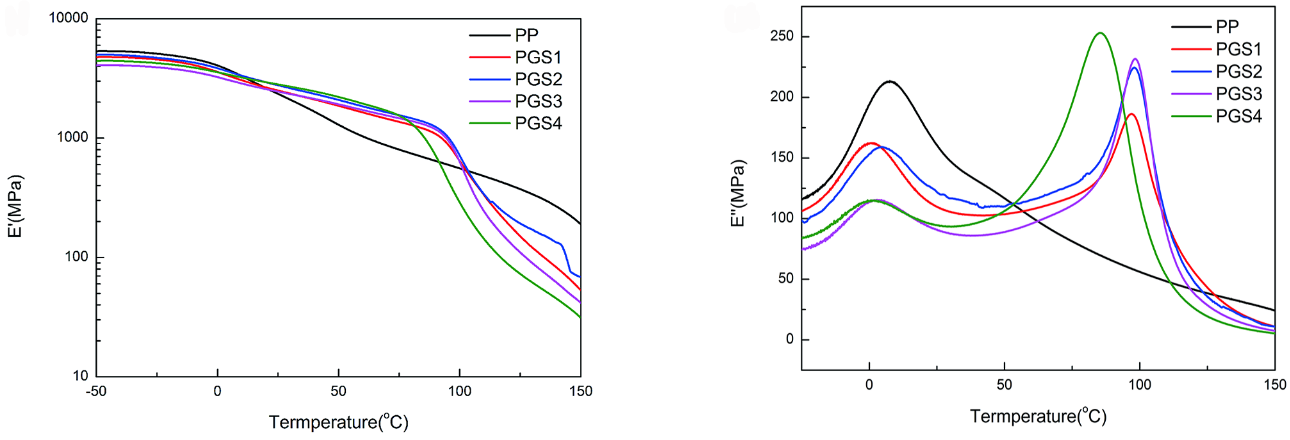

(a) (b)

Figure 4. Temperature dependence of storage modulus (a) and loss modulus (b) for PP and the graft copolymers.

Table 4. Compositions of PP/PP-g-PS blends with various copolymers.

Sample	PP	G-2.5	G-5	G-7.5	G-10	G-15
PP-*g*-PS/PP (weight ratio)	0/100	2.5/97.5	5.0/95	7.5/92.5	10/90	15/85

blending samples listed in Table 4 are named as G-2.5, G-5, G-7.5, G-10 and G-15 according to the weight percentage of PGS2.

Miscibility of PP/PP-g-PS blends

Since the connection between PP matrix and PS disperse phases is through covalent bond rather than hydrogen bond or Van der Waals forces, the interfacial adhesion of PP/PP-*g*-PS blends is much stronger than that of PP/PS blends. The present work focuses on the effect of graft copolymer composition on the performances of PP/PP-*g*-PS binary blends. Therefore, PP/PS blend with the weight ratio of 3.75/96.25(PS/PP) was prepared as a control sample, in which the PS content was equal to that of G-7.5.

The morphologies of PP/PS and PP/PP-g-PS binary blends are displayed in Figure 5. As shown, the morphology of PP/PS blend, which does not have connection through covalent bond, displays sharp interfaces and debonding. For the PP/PP-*g*-PS blends, a two-phase structure is also observed, but the interfacial phase between the PP matrix and the PS particle is obscure. However, the apparent extracting holes form during fracture, indicating a strong adhesion between the matrix and disperse phases due to the chemical bond joint. As the graft copolymer content increases, the PS dispersed phase size enlarges. In the samples of G-2.5, G-5 and G-7.5, a large number of small and uniform PS particles are observed, as the PP-*g*-PS content is up to 10%. Whereas the PS dispersed particles display bigger size and a small amount of irregular shape in G-10 and G-15. It is ascribed to the increase of grafted copolymer content advancing the chance of the PS chain entanglement and inducing the PS phase self-aggregate to form tiny particles. Though the dispersed phase particle size in G-10 and G-15 is smaller than that of PP/PS blends, the G-10 and G-10 samples present more regular shape and more obscure phase boundary than the PP/PS blends.

To quantitatively characterize the particle diameter evolvement of the PP/PS and PP/PP-*g*-PS blends, the PS particles in SEM micrograph were identified and their mean diameters were measured using Nano measurer software. The mean diameter distribution and average diameter of PS particles in each sample are shown in Figure 6. The mean diameter distribution of

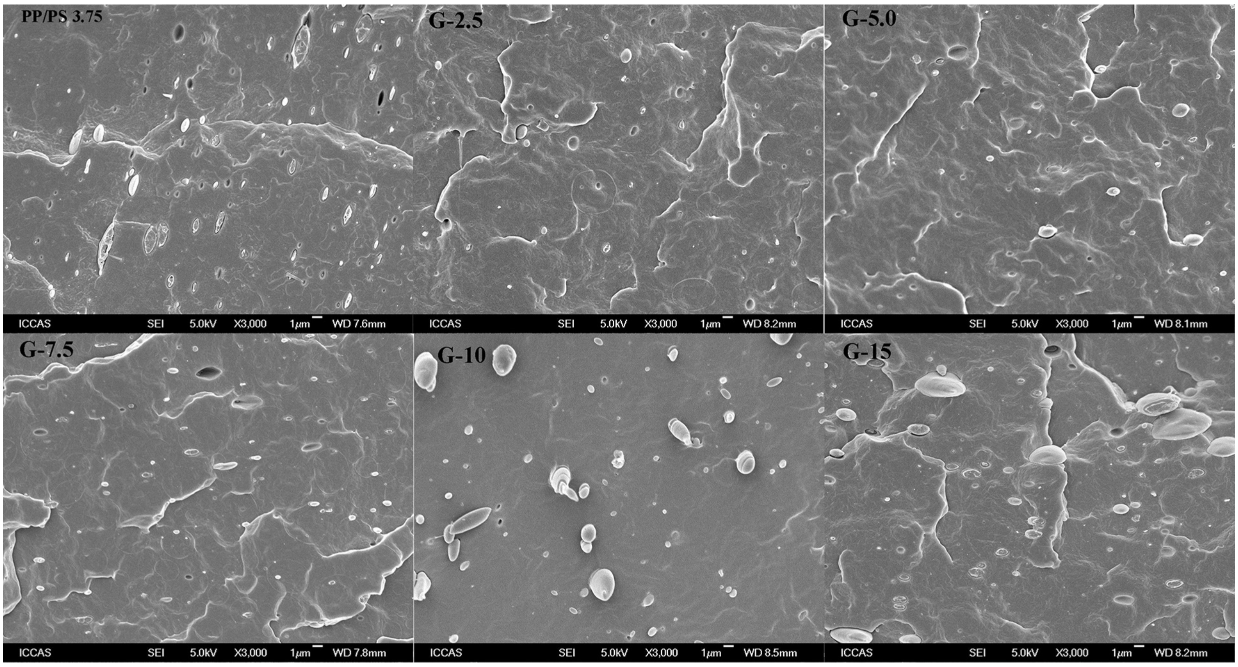

Figure 5. SEM micrographs of PP/PS and PP/PP-g-PS blends. (the scale bar is 1μm).

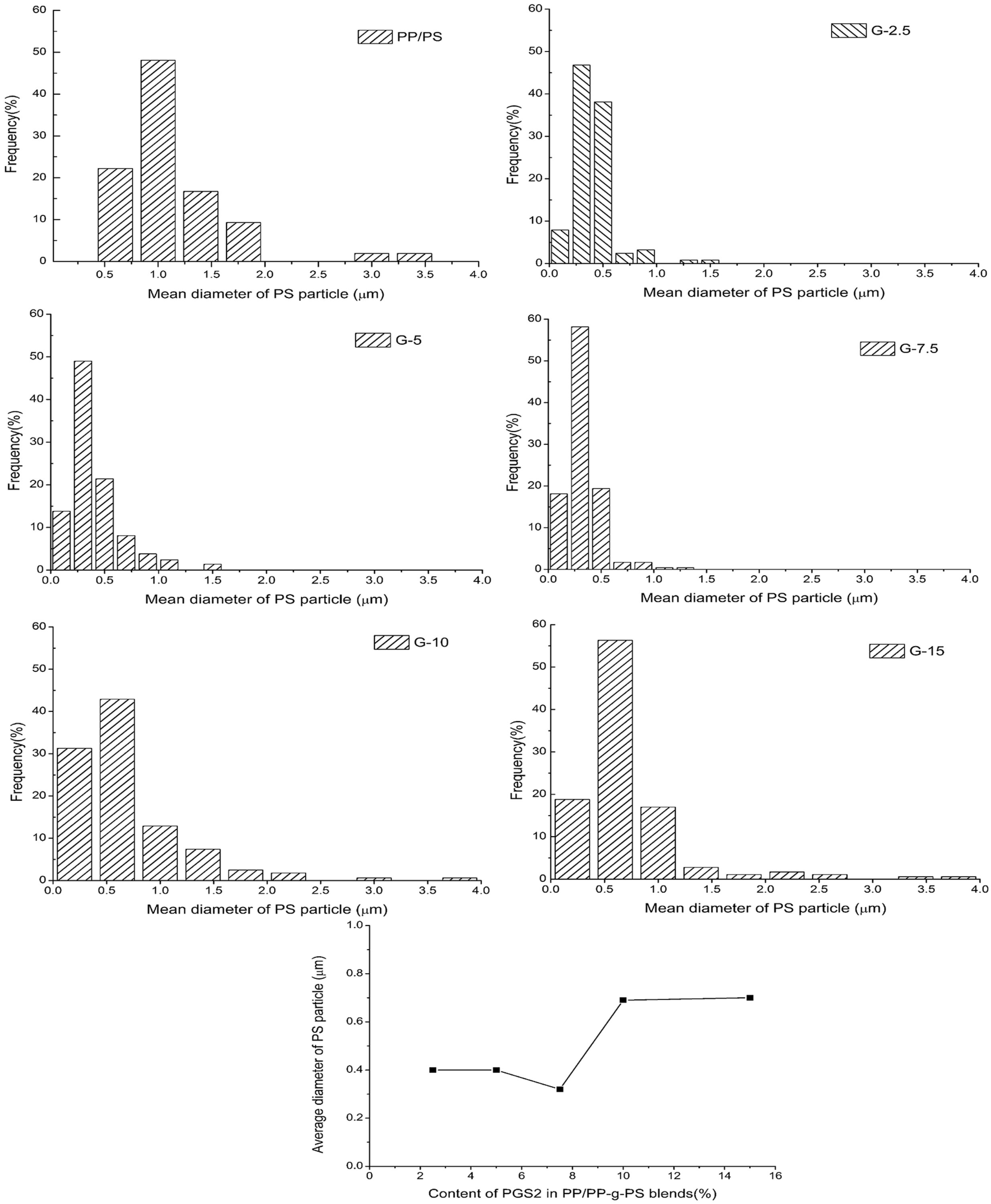

Figure 6. Diameter distributions and average diameters of PS particles of PP/PS, G-2.5, G-5, G-7.5, G-10 and G-15.

the PP/PS blends is broad, and the average diameter of PS particles is 0.92μm. As the PP-g-PS content increases, the average diameter of PS particles slightly decreases until the smallest average diameter of PS particles occurs in G-7.5, and then increases obviously. The average diameter values of samples G-2.5, G-5 and G-7.5 are less than 0.40 μm and the mean diameter distribution of these samples is narrow, while the samples G-10 and G-15 display an average diameter more than 0.70 μm and an obviously broad distribution. The crystallization ability of PP-g-PS could be dramatically affected apparently by the random PS

Table 5. Thermal properties of neat PP and PP/PP-g-PS blends.

Sample	$T_o^{(a)}$(°C)	$T_c^{(a)}$(°C)	$\Delta H_c^{(a)}$(J/g)	$X_c^{(b)}$ (%)
PP	115.2	111.7	99.1	47.4
G-2.5	125.0	122.1	102.4	49.0
G-5	125.1	121.8	100.8	48.2
G-7.5	125.7	122.4	101.0	48.3
G-10	125.4	118.7	99.7	47.7
G-15	126.4	122.9	92.1	44.1

[a] Crystallization temperature (T_c), crystallization onset temperature (T_o), and crystallization enthalpy (H_c) of each sample were registered by DSC.

[b] Relative crystallinity (X_c) was calculated by dividing the observed ΔH_c by the crystallization enthalpy of complete crystallized isotactic polypropylene (ΔH_c^0 209J/g). The contribution of the graft copolymer was not considered in the calculation of the relative crystallinity of the blends.

branched chain as described above. The thermal properties of the PP/PP-g-PS blends are listed in Table 5. Tg,PS is not detected due to the low PS content in the PP/PP-g-PS blends. The crystallization temperature of binary blends was found 10°C higher than that of neat PP, and the crystallization enthalpy and crystallinity decreased as the content of graft copolymer increased. According to D'Orazio's reports, the PP-g-PS graft copolymer plays a role of heterogeneous nucleation in the PP/PP-g-PS/PS ternary blends. Therefore, we can infer that the PP-g-PS graft copolymer plays the same role in the studied binary blends and accelerates the crystallization rate of PP in the crystallization process. Additionally, the increase of PS phase will hinder PP spherulite growth (dilution effect) especially as function of the graft copolymer increasing in the nuclei growth period, which results in the decrease of the relative crystallinity.

The crystal morphology of PP and PP/PP-g-PS blends is further studied and the isothermally crystallized optical micrography photos at 140°C are shown in Figure 7. Within the scope of observation, a typical spherulitic morphology with Maltese-cross pattern is revealed in the neat PP and binary blends. Comparing the neat PP sample, the binary blends obviously display more crystal number and smaller crystal size due to the heterogeneous nucleation of PP-g-PS.

Figure 8 shows the temperature dependence of the storage modulus and loss modulus of the neat PP and PP/PP-g-PS blends. As seen from the temperature dependence of the storage modulus, the storage modulus of the blends almost increases as a function of grafted copolymer content except for G-10. It may be related to the increase of the PS particle size in the PP matrix. This result demonstrates that the introduction of the PP-g-PS graft copolymer fraction significantly improves the rigidity of binary blends.

The mechanical properties of binary blends are directly associated with their morphology. The covalent bond between the two phases increases the compatibility and interfacial adhesion between PP and PS. Therefore, the mechanical properties of PP/PP-g-PS

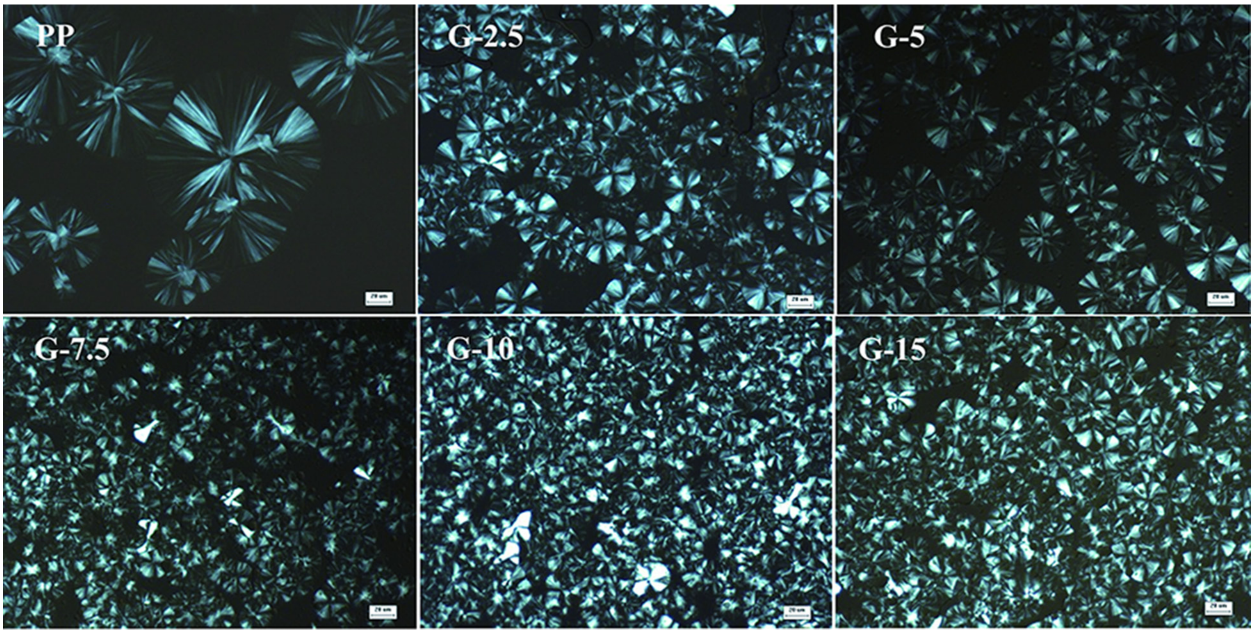

Figure 7. Optical micrographs of PP and PP/PP-g-PS blends isothermally crystallized at 140°C (the scale bar is 20μm).

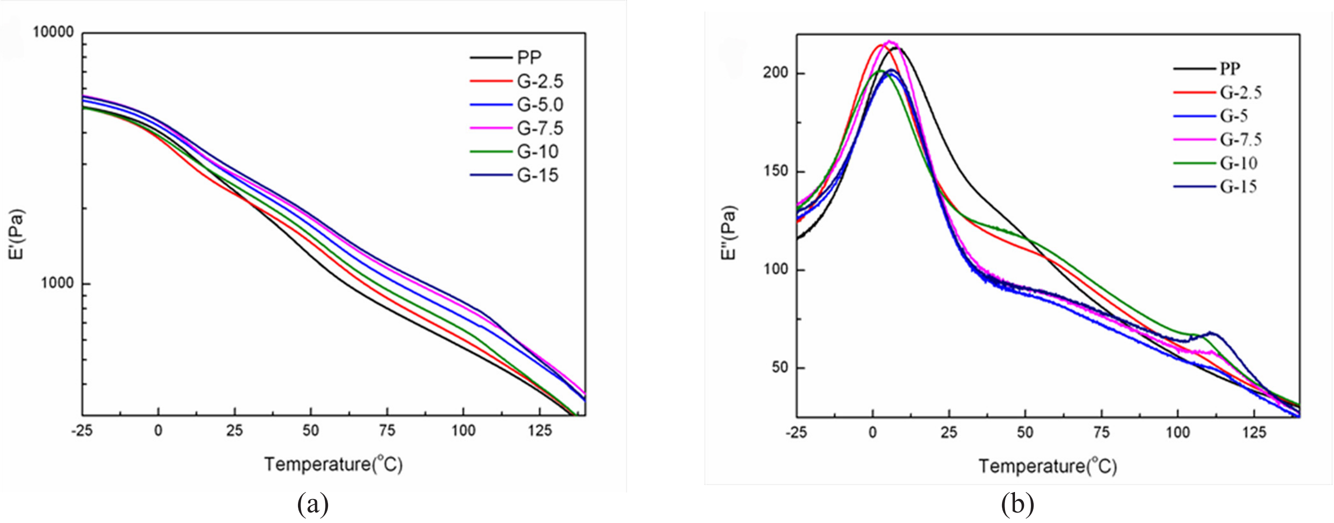

(a) (b)

Figure 8. Temperature dependence of storage modulus (a) and loss modulus (b) for PP and the PP/PP-g-PS blends.

blends could be improved. The mechanical properties of PP and PP/PP-g-PS blends are listed in Table 6. And the tensile strength, flexural modulus and impact strength of neat PP and PP/PP-g-PS blends with different PP-g-PS contents are plotted in Figure 9. As the PP-g-PS content increases, the tensile strength varies indistinctively and the flexural modulus improves apparently in the studied samples. The impact strength reaches the peak value when the PP-g-PS content is 2.5%, and then gradually drops with more introduction of PP-g-PS copolymer. The variation trends of mechanical properties display that both the rigidity and toughness of PP are improved.

Additionally, it is found that the PS particle size enlarges with the increase of the grafted copolymer contents in the blends, and a large number of small and uniform PS particle are observed in the samples G-2.5, G-5 and G-7.5. Although the rigid PS particles are introduced into PP, the graft copolymer plays a toughening role due to its uniform and small size. When the dispersion size of PS phase increases gradually, the flexural modulus raises and the impact strength decreases.

Table 6. Mechanical properties of PP and PP/PP-g-PS blends.

Sample	Tensile strength (MPa)	Flexural modulus (MPa)	Notch izod impact strength (J/m)
PP	37.39±0.58	1121±42	23.57
G-2.5	37.40±1.13	1175±9	30.73
G-5	37.20±1.09	1210±11	28.15
G-7.5	37.40±1.37	1247±11	28.03
G-10	37.66±0.78	1284±43	26.96
G-15	38.43±0.97	1293±42	25.37

CONCLUSION

PP-g-PS copolymers with increasing side chain length of PS sequences were synthesized. The crystallization rate of the graft copolymers is significantly accelerated due to the introduction of PS branch chain. The graft copolymer shows a two-phase structure and the PS branch chain hinders the formation of PP spherulites. The PP-g-PS copolymers were blended with PP to form the binary blends. The graft copolymer displays well dispersion, which promotes the crystallization process, elevates the crystallization temperature, and decreases the spherulite size of PP. The formation of covalent bond between the two phases improves the compatibility and interfacial adhesion between PP and

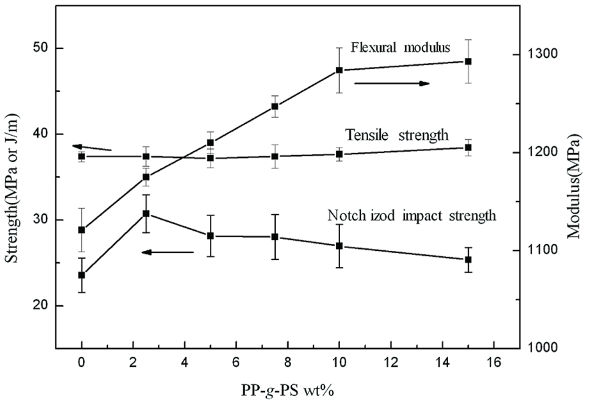

Figure 9. Mechanical properties of PP and PP/PP-g-PS.

PS. And the tensile modulus and impact strength of PP/PP-g-PS blends are also obviously improved.

ACKNOWLEDGEMENTS

The authors thank the financial support from the National Science Foundation of China (Grant No. 51343006 & 51403216).

REFERENCES

1. Danella OJ, Manrich S (2003) Morphological study and compatibilizing effects on polypropylene/polystyrene blends. Polym Sci-A 45: 1086-1092
2. Ghosh A, Sciamanna SF, Dahl JE, Liu S, Carlson RMK, Schiraldi DA (2007) Effect of nanoscale diamondoids on the thermomechanical and morphological behaviors of polypropylene and polycarbonate. J Polym Sci Pol Phys 45: 1077-1089
3. Yin ZH, Zhang XM, Zhang YJ, Yin JH (1997) Morphological, thermal, and mechanical properties of polypropylene/polycarbonate blend. J Appl Polym Sci 63: 1857-1863
4. Adewole AA, Denicola A, Gogos CG, Mascia L (2000) Compatibilization of polypropylene - Polystyrene blends: Part 2, crystallization behavior and mechanical properties. Adv Polym Tech 19: 180-193
5. Adewole AA, DeNicola A, Gogos CG, Mascia L (2000) Compatibilisation of polypropylene-polystyrene blends - Part 1 - Effect of mixing intensity on morphology and rheological properties. Plast Rubber Compos 29: 70-79
6. Caporaso L, Iudici N, Oliva L (2005) Synthesis of well-defined polypropylene-graft-polystyrene and relationship between structure and the ability to compatibilize the polymeric blends. Macromolecules 38: 4894-4900
7. Diaz MF, Barbosa SE, Capiati NJ (2005) Improvement of mechanical properties for PP/PS blends by in situ compatibilization. Polymer 46: 6096-6101
8. Wang Y, Ma CB, Sheng J (2008) Study of morphology and mechanical properties of in situ PP/PS alloy. J Macromol Sci Phys 47: 117-126
9. Li JG, Li HY, Wu CH, Ke YC, Wang DJ, Li Q, Zhang LY, Hu YL (2009) Morphologies, crystallinity and dynamic mechanical characterizations of polypropylene/polystyrene blends compatibilized with PP-g-PS copolymer: Effect of the side chain length. Eur Polym J 45: 2619- 2628
10. Zhou Q, Zheng T, Li H, Li Q, Zhang Y, Zhang L, Hu Y (2014) Effects of some new alkoxysilane external donors on propylene polymerization in $MgCl_2$-supported Ziegler-Natta catalysis. Ind Eng Chem Res 53: 17929-17936
11. Wang L, Jiang ZW, Liu F, Zhang ZJ, Tang T (2014) Effects of branches on the crystallization kinetics of polypropylene-g-polystyrene and polypropylene-g-poly(n-butyl acrylate) graft copolymers with well-defined molecular structures. Chinese J Polym Sci 32: 333-349
12. Mucha M, Marszalek J, Fidrych A (2000) Crystallization of isotactic polypropylene containing carbon black as a filler. Polymer 41: 4137-4142
13. Peng H, Luo Y, Hong H, Liu L, Jia D (2008) Study on crystallization behavior of solid-phase graft copolymers of polypropylene with maleic anhydride and methyl methacrylate. Polym Plast Technol Eng 47: 996-1001